NJC

Accepted Manuscript

This is an *Accepted Manuscript*, which has been through the Royal Society of Chemistry peer review process and has been accepted for publication.

Accepted Manuscripts are published online shortly after acceptance, before technical editing, formatting and proof reading. Using this free service, authors can make their results available to the community, in citable form, before we publish the edited article. We will replace this *Accepted Manuscript* with the edited and formatted *Advance Article* as soon as it is available.

You can find more information about *Accepted Manuscripts* in the Information for Authors.

Please note that technical editing may introduce minor changes to the text and/or graphics, which may alter content. The journal's standard Terms & Conditions and the Ethical guidelines still apply. In no event shall the Royal Society of Chemistry be held responsible for any errors or omissions in this *Accepted Manuscript* or any consequences arising from the use of any information it contains.

ROYAL SOCIETY OF CHEMISTRY

www.rsc.org/njc

Journal Name

RSC Publishing

ARTICLE

Visible light-induced enhanced photoelectrochemical and photocatalytic studies of gold decorated SnO_2 nanostructures†

Cite this: DOI: 10.1039/x0xx00000x

Received 00th January 2012,
Accepted 00th January 2012

DOI: 10.1039/x0xx00000x

www.rsc.org/

Mohammad Mansoob Khan[1¥], Sajid Ali Ansari[1], Mohammad Ehtisham Khan[1], Mohd Omaish Ansari[1], Bong-Ki Min[2] and Moo Hwan Cho[1]*

This paper reports the novel one-pot biogenic synthesis of Au-SnO_2 nanocomposite using electrochemically active biofilms. The synthesis, morphology and structure of the as-synthesized Au-SnO_2 nanocomposite was in-depth studied and confirmed by UV-vis spectroscopy, photoluminescence spectroscopy, transmission electron microscopy, X-ray diffraction, and X-ray photoelectron spectroscopy. It was observed that SnO_2 surface was decorated homogeneously with Au nanoparticles. The photoelectrochemical behavior of the Au-SnO_2 nanocomposite was examined by cyclic voltammetry, differential pulse voltammetry, electrochemical impedance spectroscopy, and linear sweep voltammetry in the dark and under visible light irradiation. Visible light-induced photoelectrochemical studies confirmed that the Au-SnO_2 nanocomposite had enhanced activities compared to the P-SnO_2 nanoparticles. The Au-SnO_2 nanocomposite was also tested for the visible light-induced photocatalytic degradation of Congo red and methylene blue, and showed approximately 10 and 6 fold higher photocatalytic degradation activity, respectively, compared to P-SnO_2. These results showed that the Au-SnO_2 nanocomposite exhibits excellent and higher visible light-induced photoelectrochemical and photocatalytic activities than the P-SnO_2 nanoparticles, and can be used for a range of applications.

Introduction

Tin oxide (SnO_2) nanocrystals have various applications, such as transparent conductors, gas sensing, photocatalysis, energy storage and conversions.[1-4] The behavior of SnO_2 nanocrystals is size dependent, which can provide an interface for the interaction between SnO_2 and other species, leading to enhanced performance in photocatalysis, capacitance and sensing.[1-5] SnO_2 has been used as a photocatalyst and electrode material on account of its high chemical stability, surface area and comparatively high capacitive behavior.[3,4] These properties make SnO_2 a good choice for potential electrode materials and photocatalysts in the field of nanocomposites synthesis.

Gold nanoparticles (AuNPs) have desirable properties, such as strong surface plasmon, catalysis and redox behaviors.[6-8] AuNPs are also well known for quantized capacitance charging.[8-10] This is achieved by the electron storage and quantized capacitance charging characteristics of AuNPs.[9,11] Previous studies have established that several hundred electrons can be stored on AuNPs in solution; hence AuNPs can also provide a surface for different types of catalytic reactions.[5-9] Electrochemistry, as a means of charging AuNPs, has been studied extensively since Murray's revolutionary work on quantized capacitance charging.[10]

Recently, composite materials of SnO_2, such as Au@SnO_2, Ag@SnO_2, graphene/SnO_2, Sb-SnO_2, have been reported for a range of applications.[12-23] Among them, Au@SnO_2 nanocomposites are believed to show high capacitance, sensing and catalytic activities.[3,5,12-16] Recent studies have focused on alternative low cost transition metal-metal oxide (SnO_2) nanocomposites because of their high energy density, environmental compatibility and natural abundance.[5,22] On the other hand, SnO_2 shows low capacitance and catalytic activity without conducting additives because of its intrinsically poor electrical conductivity.[21,22] Some studies have reported the benefits of using metal nanoparticles to improve the charging, capacitance and catalytic activities of SnO_2.[5,22]

Therefore, in the present study, the reported biogenic and green approach was extended to the synthesis of Au-SnO_2 nanocomposite.[6,18] In comparison to previous reports, the as-synthesized Au-SnO_2 nanocomposite was in-depth characterized and studied using XRD through Rietveld refinement in the 20 – 140° 2θ range, TEM via inverse fast Fourier transform (IFFT), elemental mapping of elements and X-ray photoelectron spectroscopy (XPS)

analysis.[18,27] The main aim of this study was to enhance the visible light activity of P-SnO_2 by anchoring AuNPs on the SnO_2 surface, and thorough explore their visible light-induced photoelectrochemical properties using techniques, such as cyclic voltammetry (CV), differential pulse voltammetry (DPV), electrochemical impedance spectroscopy (EIS), and linear sweep voltammetry (LSV) for possible applications in capacitance, quantized capacitance charging and as an effective photoelectrode material. The advantage of the photoelectrochemical method is that it is highly sensitive, relatively inexpensive and can be used to give the desired results within a short time interval under normal conditions. The as-synthesized Au-SnO_2 nanocomposite was also tested for the photocatalytic degradation of Congo red (CR) and methylene blue (MB) under visible light irradiation to assess the visible light-induced photocatalytic activity. The as-synthesized Au-SnO_2 nanocomposite exhibited enhanced visible light-induced photoelectrochemical responses and photocatalytic degradation of CR and MB, which may give better understanding of the novel properties exhibited by the Au-SnO_2 nanocomposite.

Experimental

Materials

Tin oxide nanoparticles (SnO_2; <100 nm particle size, BET) were obtained from Sigma–Aldrich, whereas hydrogen tetrachloroaurate (III) hydrate ($HAuCl_4{\cdot}nH_2O$; n = 3.7) was purchased from Kojima Chemicals, Japan. CH_3COONa, Na_2SO_4, Na_2HPO_4, and NaH_2PO_4 were obtained from Duksan Pure Chemicals Co. Ltd. South Korea. Ethyl cellulose and α-terpineol were purchased from KANTO Chemical Co., Japan, whereas fluorine-doped transparent conducting oxide glass (FTO; F-doped SnO_2 glass; 7 Ω/sq) was supplied by Pilkington, USA. Carbon paper (without wet proof) was obtained from Fuel Cell Earth LLC, USA. All other chemicals used in this study were of analytical grade and used as received. All the solutions for the synthesis, photoelectrochemical and photocatalytic studies were prepared in deionized (DI) water, which was obtained using a PURE ROUP 30 water purification system.

Methods

An UV-VIS-NIR spectrophotometer (Cary 5000, VARIAN, USA) was used to record the diffuse reflectance/absorbance spectra (DRS) of the Au-SnO_2 nanocomposite and P-SnO_2 nanoparticles. The photoluminescence (PL, Kimon, 1 K, Japan) spectra of the Au-SnO_2 nanocomposite and P-SnO_2 nanoparticles were recorded over the range, 200-800 nm, at an excitation wavelength of 325 nm and a power of 50 mW. X-ray diffraction (XRD, PANalytical, X'pert PRO-MPD, Netherland) was carried out using Cu Kα radiation (λ = 0.15405 nm). A Rietveld refinement was conducted using Muad 2.46 software. X-ray photoelectron spectroscopy (XPS, ESCALAB 250 XPS System, Thermo Fisher Scientific U.K.) was performed using monochromatized Al Kα x-rays (hν = 1486.6 eV). The binding energy of C 1s (284.60 eV) was used to calibrate the other binding energies. PL and XPS were performed at the Korea Basic Science Institute (KBSI), South Korea. The samples for TEM analysis were prepared by dispersing the materials in ethanol by an ultrasonic treatment for 5 minutes (CPX2800H-E, Branson Ultrasonic Corporation, USA) and then dropped onto ultrathin carbon covered copper grids. The microstructure, size and distribution of the Au-SnO_2 nanocomposite and P-SnO_2 nanoparticles were observed by field emission transmission electron microscopy (FE-TEM, Tecnai G2 F20, FEI, USA) with an accelerating voltage of 200 kV combined with energy dispersive spectrometry (EDS) and high angle annular dark field STEM (HAADF-STEM). The Brunauer–Emmett–Teller (BET) specific surface area of the powder samples were measured using a Chem BET TPR/TPD analyzer (Quantachrome, Inc) equipped with a thermal conductivity detector. Before the BET measurement, samples were degassed at 150 ^oC in N_2 condition. The photoelectrochemical and photocatalytic experiments were carried out using a 400 W lamp (3 M, USA) with λ > 400 nm and an intensity of 31 mW/cm^2.

CV of the Au-SnO_2 and P-SnO_2 photoelectrodes was conducted in a 0.1 M phosphate buffer solution (PBS, pH 7). DPV of the Au-SnO_2 and P-SnO_2 photoelectrodes was performed with a pulse height of 50 mV, pulse width of 0.005 s and scan rate of 4 mV/s in 0.1 M PBS. The EIS and LSV of the photoelectrodes prepared by the Au-SnO_2 nanocomposite and P-SnO_2 nanoparticles were performed in a three electrode cell with an aqueous 0.2 M Na_2SO_4 solution as the electrolyte using a potentiostat (VersaSTAT 3, Princeton Research, USA). The working electrodes were prepared by taking 100 mg of the Au-SnO_2 nanocomposite or P-SnO_2 nanoparticles and mixing it thoroughly with ethyl cellulose, as the binder, using a conditioning mixer and adding α-terpineol, as a solvent, to make a paste. The resulting paste was then coated on a FTO glass substrate using the doctor-blade method. The projection area of each electrode was 0.64 cm^2. The Au-SnO_2 nanocomposite and P-SnO_2 nanoparticles-coated (FTO) glass substrates were used as the working electrode. Ag/AgCl (3.0 M KCl) and a Pt gauge were used as the reference and counter electrodes, respectively.

Electrochemically active biofilm development

A mixed cultured EAB was developed on plain carbon paper according to previous reports.[6,8,24,25] In a typical procedure, 10 mL of anaerobic sludge (from a biogas plant in Paju, Korea) was added to a mineral salt medium (200 mL) containing sodium acetate (1 g/L) as a substrate in a 250 mL reaction bottle. N_2 gas was sparged for 5 min to remove the dissolved oxygen and create an inert atmosphere. Carbon paper, 2.5 cm × 4.5 cm in size, was then dipped into the solution. All media, including the bacterial inoculum, were changed every two days under strict anaerobic conditions. This process was repeated for two weeks, which gave an active EAB developed on the surface of the carbon paper. The developed EAB was used to synthesize the nanocomposite.

EAB assisted synthesis of Au-SnO_2 nanocomposite

The EAB developed on carbon paper was used to synthesize the Au-SnO_2 nanocomposite. In a normal process, an aqueous solution of hydrogen tetrachloroaurate (III) hydrate (1 mM) was added to a 200 mL suspension of SnO_2 nanoparticles (4 mM) and stirred magnetically for 5 minutes to allow the adsorption of $AuCl_4^-$ ions on the surface of the SnO_2 nanoparticles. Subsequently, 0.2 g sodium acetate (1 g/L) was added as an electron donor and N_2 gas was sparged. An EAB was then hung in a reaction flask. The EAB produced electrons under anaerobic conditions, which was then used for the reduction of Au^{3+} ions to Au^0 at the P-SnO_2 surface. The initial golden yellow color changed after 18 h to a purple color, which is indicative of the formation of Au-SnO_2 nanocomposite in solution. The solution was then centrifuged to isolate the Au-SnO_2 nanocomposite, which have a purple color. The isolated powdered Au-SnO_2 nanocomposite was dried in an oven at 60 °C for 20 h, and later stored in a desiccator for various studies.

In addition, two control experiments were performed to check and confirm the roles of both the EAB and sodium acetate in the synthesis. First, a controlled experiment was performed in the absence of an electron donor, i.e., sodium acetate, in which only the developed EAB was hung in the SnO_2 suspension and a hydrogen tetrachloroaurate (III) hydrate solution was then added under anaerobic conditions. The second controlled experiment was performed in the absence of the EAB by adding only the electron donor (sodium acetate) in a SnO_2 suspension and chloroauric acid mixture under anaerobic conditions. In both controlled experiments, no color change was observed, even after 36 h. These experiments confirmed the roles of both sodium acetate and EAB in the synthesis of the Au-SnO_2 nanocomposite.

Photoelectrochemical studies (CV, DPV, EIS and LSV)

The photoelectrochemical behavior of Au-SnO_2 nanocomposite and P-SnO_2 nanoparticles was examined by CV, DPV, EIS and LSV carried out under ambient conditions in the dark and under visible light irradiation. The CV and DPV experiments were performed in 50 mL of a 0.1 M PBS in the dark and under visible light irradiation. CV was performed at a scan rate of 50 mV/s, whereas DPV was measured at pulse height, pulse width, and scan rate of 50 mV, 0.005 s, and 4 mV/s respectively. The EIS and LSV experiments were performed in 50 mL of an aqueous 0.2 M Na_2SO_4 solution in the dark and under visible light irradiation at room temperature. EIS was performed in the dark, and later under visible light irradiation (λ > 400 nm) with frequencies ranging from 1 – 10^4 Hz at 0.0 V vs. Ag/AgCl in potentiostatic mode. The photocurrent response was examined by LSV in the dark and under visible light irradiation at a scan rate of 50 mV/s over the potential range of -1.0 to 1.0 V.

Photocatalytic degradation of dyes

The visible light-induced photocatalytic degradation activities of the as-synthesized Au-SnO_2 nanocomposite and P-SnO_2 nanoparticles were tested for the degradation of CR and MB under visible light irradiation. The photocatalytic activities were measured by the photodecomposition of CR and MB at a concentration of 10 mg/L each. For the photodecomposition reaction, 3 mg of each photocatalyst was suspended in 20 mL of aqueous solutions of CR or MB followed by sonication for 10 min in the dark. The solutions were stirred in the dark again for 30 min to complete the adsorption and desorption equilibrium of the specific substrate on the Au-SnO_2 nanocomposite and P-SnO_2 nanoparticles. Visible light irradiation of the solutions were performed using a 400 W lamp (λ > 400 nm). Both CR and MB degradation experiments were conducted for 4 h. Dye degradation was monitored by taking 1.7 mL of the degraded samples at 1 h intervals using a micropipette from each set, centrifuging it to remove the catalyst and then recording the UV–vis spectrum. The degradation of CR and MB was calculated from the decrease in the absorbance of the degraded solutions. Each experiment was conducted in triplicate to ensure the reliability of the photocatalytic degradation activities of the Au-SnO_2 nanocomposite and P-SnO_2 nanoparticles.

Results and discussion

The EAB was used as a green and biogenic tool to produce the Au-SnO_2 nanocomposite, which is a low-cost and environment-friendly pathway. EABs are well known in microbial fuel cells and nanomaterial syntheses.[6,8,24,25] The EAB delivers an excess of electrons by biologically decomposing the sodium acetate under anaerobic conditions.[6,8,24] The produced electrons reduce the Au^{3+} ions to Au^0 on the surface of the SnO_2 nanoparticles, which leads to the formation of Au-SnO_2 nanocomposite (Fig. 1). The two controlled experiments showed that both the EAB and sodium acetate (electron donor) are needed to complete the reaction. The advantage of this protocol is that it generally takes place in water at room temperature under atmospheric pressure, and does not involve a surfactant, capping agents and external energy input. The product obtained in this synthesis was extracellular (outside of the bacterial cells) and pure, as the biofilm was supported on carbon paper. This also minimizes the impurities and reduces the number of synthetic steps. These advantages make this synthesis quite useful and efficient for the synthesis of various types of nanocomposites.

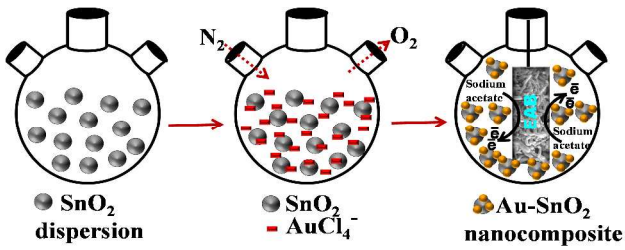

Fig. 1 Proposed schematic model for the synthesis of Au-SnO_2 nanocomposite using an EAB.

Optical studies

The light absorption characteristics of any powdered material can be examined by UV-visible diffuse reflectance/absorbance spectroscopy. Fig. 2a shows the UV–vis diffuse absorption spectra of the Au-SnO_2 nanocomposite and P-SnO_2 while the inset shows the color of the samples. Fig. S1 shows their diffuse reflectance spectra.

The spectrum of P-SnO_2 shows that it absorbs light mainly in the UV region of the spectrum because of its wide band gap, whereas the spectrum of the Au-SnO_2 nanocomposite showed a broad absorption peak from 500-600 nm in the visible region of the spectrum, which was assigned to the surface plasmon resonance absorption of the AuNPs.[6-8,14,20] When SnO_2 was decorated with AuNPs, the nanocomposite developed a purple color due to the characteristic surface plasmon band of gold.[17] This confirms that the AuNPs decorated the surface of P-SnO_2 effectively. In case of Au-SnO_2 nanocomposite a shift in the absorption edge (250 – 350 nm) was observed in comparison to the P-SnO_2 which can be attributed to the anchoring of AuNPs at P-SnO_2 surface.[17,20] In addition, the absorption edge shift and high absorption in 400 – 600 nm range suggests an interfacial interaction between the Au and P-SnO_2 nanoparticles, which is also in agreement with the other characterization techniques.

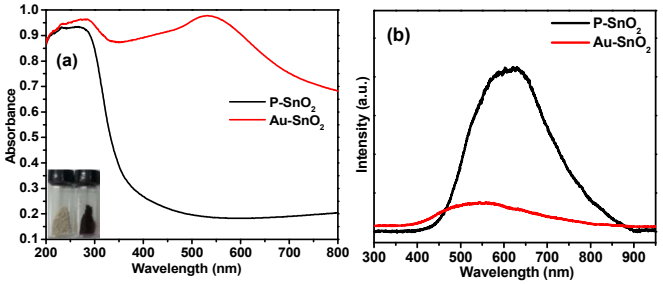

Fig. 2 (a) UV-vis diffuse absorption spectra, and **(b)** PL spectra of the Au-SnO_2 nanocomposite and P-SnO_2 nanoparticles.

Fig. 2b shows the PL spectra of the Au-SnO_2 nanocomposite and P-SnO_2 nanoparticles. The intensity of the PL spectrum is related directly to the electron-hole recombination rate, *i.e.*, more intense the spectrum, the higher the rate of electron-hole recombination.[26,27] On the other hand, a lower intensity indicates that more excited electrons are trapped and transferred gradually through the interface.[27] The Au-SnO_2 nanocomposite showed reduced PL emission intensity compared to P-SnO_2, which exhibited strong PL emission intensity. The PL intensity in the case of the Au-SnO_2 nanocomposite was reduced significantly after decoration with the AuNPs because Au can trap photo-generated electrons to facilitate charge separation.[26,27] In general, the efficient charge separation and the inhibited electron-hole recombination by the AuNPs are favorable for enhancing the photo-activity of P-SnO_2. The PL spectra showed that a AuNPs decoration of the P-SnO_2 surface can effectively inhibit electron-hole recombination during visible light irradiation. This further confirms the enhanced visible light activities of the Au-SnO_2 nanocomposite.

Structural, morphological and compositional studies

Fig. S2 presents XRD patterns of the Au-SnO_2 nanocomposite and P-SnO_2 nanoparticles in the 20 – 90° 2θ range, in which two sets of XRD patterns are shown. The peaks at 37.78°, 44.13°, 64.27°, and 78.27° 2θ marked with "*" were assigned to the (111), (200), (220) and (311) planes of face centered cubic (fcc) Au (JCPDS No. 04-0784).[27,28] The unmarked peaks were indexed to the crystalline tetragonal structure of SnO_2 (JCPDS No. 41-1445).[13-15,28] The XRD findings were further confirmed using a "Rietveld refinement", as shown in Fig. 3. The Rietveld refinement is a simple tool to verify the precise structure of the Au-SnO_2 nanocomposite and P-SnO_2 nanoparticles, and quantify the phase fraction (Table 1). For Rietveld refinement XRD was performed in 20 – 140° 2θ range. Using this method, the structural composition of each sample was analyzed qualitatively by fitting the experimental powder XRD profiles with respect to the corresponding structural parameter (i.e. lattice parameters, atomic coordinates) and instrumental parameters (i.e. zero-point and profile parameters), as listed in Table 1. Fig. 3b shows the standard peaks of Au (JCPDS No. 04-0784) and SnO_2 (JCPDS No. 41-1445) in the bottom. The Rietveld refinement further confirmed the synthesis of the Au-SnO_2 nanocomposite. The refinement was converted to the final residual factors (Fig. S3) of R_{wp} = 6.46 %, R_{exp} = 4.39 % and χ^2 = 2.16 for the P-SnO_2 nanoparticles, and R_{wp} = 6.46 %, R_{exp} = 4.41 % and χ^2 = 2.14 for the Au-SnO_2 nanocomposite, where R_{wp} is the weighted-profile R value, R_{exp} is the statistically expected R value and χ^2 is the goodness of fit, which is the square of the ratio between R_{wp} and R_{exp}.

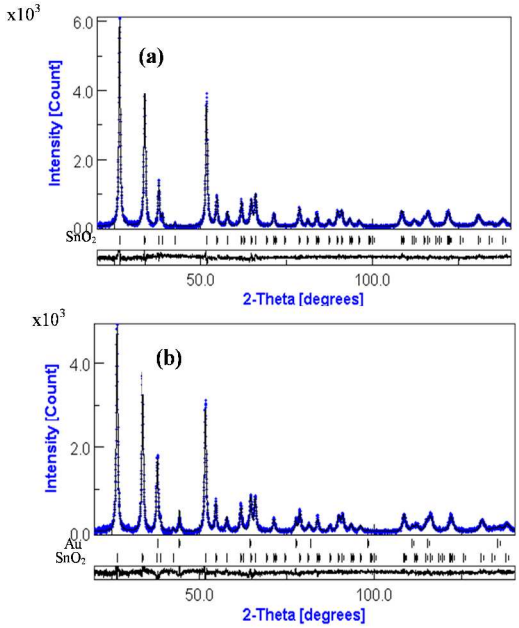

Fig. 3 XRD patterns of the (**a**) P-SnO_2 nanoparticles, and (**b**) Au-SnO_2 nanocomposite obtained after the "Rietveld refinement".

Table 1. Structural parameters measured from the XRD patterns of the Au-SnO_2 nanocomposite and P-SnO_2 nanoparticles after the Rietveld refinement.

S. No.	Sample	Phase	Phase fraction	Crystallite size(Å)	Cell parameter(Å)		V(Å^3)
					a	c	
1.	P-SnO_2	Rutile	1.0	232.0	4.7371	3.1863	71.276
2. Au-SnO_2	SnO_2	Rutile	0.984	244.4	4.7040	3.1884	66.052
	Au	Fm3m	0.016	190.1	4.081972		

The Rietveld refinement of the XRD data of the Au-SnO_2 nanocomposite and P-SnO_2 nanoparticles showed that after the

AuNPs decoration on the SnO_2 surface, the unit cell volume of SnO_2 in the Au-SnO_2 nanocomposite decreased by approximately 7.3% compared to the P-SnO_2 (Table 1). The decrease in unit cell volume was attributed to the development of strain or stress on the SnO_2 crystals during Au-SnO_2 synthesis, which is believed to be responsible for the decrease in the unit cell volume.[28] In case of the Au-SnO_2 nanocomposite, the crystallite size of the overall Au-SnO_2 nanocomposite increased approximately 5% compared to the P-SnO_2 (Table 1), which could be because of the AuNPs decoration on the different facets of the SnO_2 surface.[28]

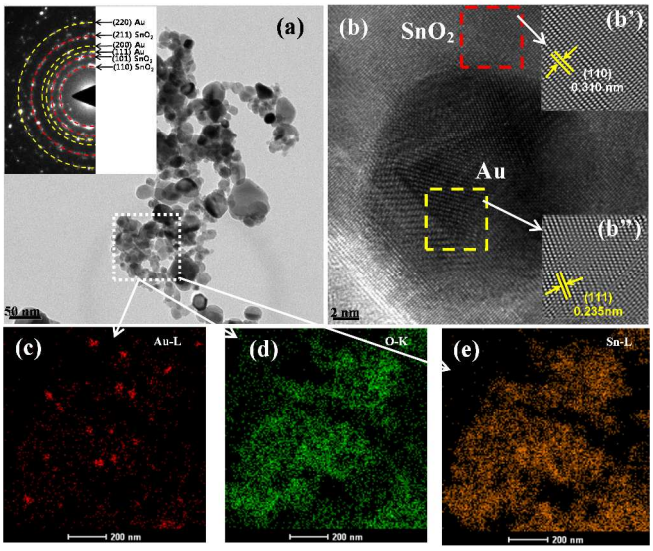

Fig. 4. (**a**) TEM image and inset shows the SAED pattern, (**b**) HR-TEM image, inset (b') shows the IFFT of SnO_2 and (b'') shows the IFFT of AuNPs, and (**c - e**) EDX elemental mapping images of the Au-SnO_2 nanocomposite.

Fig. 4 shows the TEM and high resolution-transmission electron microscopy (HR-TEM) images, as well as the selected area electron diffraction (SAED) pattern, inverse fast Fourier transform (IFFT) and mapping of the Au-SnO_2 nanocomposite to confirm the microstructure. The size of the SnO_2 nanoparticles was in the range of 25 to 30 nm (Fig. S4). Fig. S5 shows the HAADF-STEM image of the Au-SnO_2 nanocomposite. The difference in contrast (Fig. 4a) suggested that the AuNPs were well dispersed over the SnO_2 surface. This finding was further confirmed by SAED (inset of Fig. 4a) and EDS analysis (Fig. S6, see ESI†) of different regions of the Au-SnO_2 nanocomposite. The AuNPs appears to be dispersed relatively uniformly and decorated the SnO_2 surface, forming an Au-SnO_2 nanocomposite. The inset in Fig. 4a shows the SAED pattern of the Au-SnO_2 nanocomposite, suggesting that the sample has a polycrystalline structure, which is in accordance with the XRD patterns (Fig. 3). Two phases were observed with face centered cubic (fcc) lattices; Au (yellow dotted line), and the tetragonal structure of SnO_2 (red dotted line). Fig. 4b shows the typical profile view of the HR-TEM image of the AuNPs decorated on the SnO_2 matrix. HR-TEM revealed the AuNPs decoration of the SnO_2 surface along with an interface with a continuity of lattice fringes between the AuNPs and SnO_2. The inset in Fig. 4b shows the IFFT of SnO_2 (b') and AuNPs (b''), which clearly shows the 0.310 nm (110) plane of SnO_2 and the 0.235 nm (111) plane of AuNPs. As shown in Fig. 4b, the size of the AuNPs is in the range, 12−18 nm, suggested that during the formation of the Au-SnO_2 nanocomposite, the AuNPs were dispersed uniformly over the surface of the SnO_2. In other words, the AuNPs are robust enough to resist significant aggregation during the formation of the Au-SnO_2 nanocomposite and are coated uniformly over the surface of the SnO_2. This suggests that the fundamental nature of noble metal nanoparticles plays a key role in the formation of Au-SnO_2 nanocomposite.

To further examine the elemental distribution of the Au-SnO_2 nanocomposite, the elemental mapping of Au, Sn and O were also performed by EDS area scanning, as shown in Fig. 4c – e. The AuNPs were distributed homogeneously over the SnO_2 surface. The mapping of Au, Sn and O were well-defined with sharp contrast. These results provide solid evidence that SnO_2 surface was decorated successfully by Au. In addition, the EDS spectrum shows that the product contained Au as well as Sn and O (Fig. S6, see ESI†), which further confirms the formation of the Au-SnO_2 nanocomposite.

XPS was used to examine the chemical states and surface composition of the Au-SnO_2 nanocomposite and P-SnO_2 nanoparticles. The XPS survey spectra of the Au-SnO_2 nanocomposite (Fig. 5a) revealed three major sets of peaks for the Sn 3d peaks, O 1s peaks and Au 4f peaks, whereas the XPS survey spectra of the P-SnO_2 nanocomposite (Fig. 5a) revealed two major sets of peaks for the Sn 3d and O 1s peaks, which exist in the samples. No trace of impurities were observed. The carbon peak in Fig. S7 (C 1s = 284.8 eV) was assigned to the hydrocarbons from the XPS instrument and residual carbon from the sample. The XP spectra of Sn 3d, O 1s and Au 4f (Fig. 5b, c and d) revealed slightly different binding energies in the case of the Au-SnO_2 nanocomposite compared to the reported values of individual AuNPs and SnO_2, suggesting a strong interaction between the Au and SnO_2 nanoparticles.[27,29,30] Moreover, two XPS peaks (Fig. 5b) for the Sn $3d_{5/2}$ and Sn $3d_{3/2}$ core level states of Sn centered at 486.5 and 494.9 eV, respectively, corresponds to the binding energy of Sn^{4+} in SnO_2 [29].

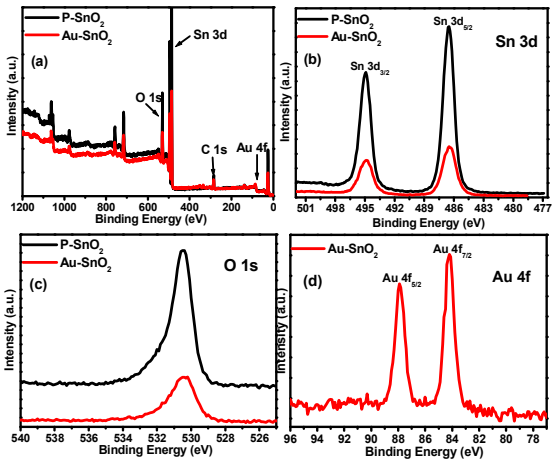

Fig. 5 XP spectra of the Au-SnO_2 nanocomposite and P-SnO_2 nanoparticles (**a**) survey spectra, (**b**) Sn 3d peaks, (**c**) O 1s peaks, and (**d**) Au 4f peaks.

In Fig. 5c, the O 1s spectra of the Au-SnO_2 nanocomposite and P-SnO_2 nanoparticles showed a single symmetrical peak at approximately 530.46 ± 0.05 eV, corresponding to the lattice oxygen of SnO_2 nanoparticles.[29] Fig. 5d shows the two individual photoelectron peaks of Au 4f; 84.10 ± 0.02 eV for Au $4f_{7/2}$ and 87.80 ± 0.02 eV for Au $4f_{5/2}$.[29] The 3.70 eV difference between the binding energy of these photoelectron peaks is also a characteristic of metallic Au, which is further evidence of the reduction of Au^{3+} ions to the Au^0 state by the EAB.[27,29,30] XPS further confirmed the decoration of the SnO_2 surface by AuNPs.

Photoelectrochemical studies of the Au-SnO_2 and P-SnO_2 photoelectrodes

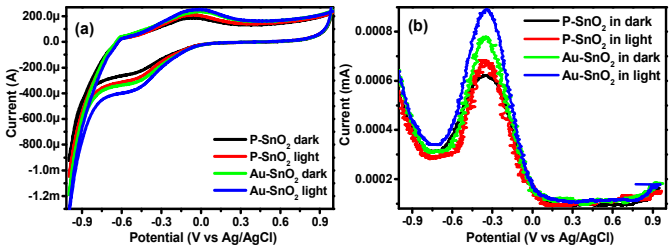

Fig. 6 Visible light-induced response of **(a)** CV, and **(b)** DPV for the Au-SnO_2 and P-SnO_2 photoelectrodes in the dark and under visible light irradiation.

Cyclic voltammetry (CV) is a powerful tool in the field of electrochemistry and is the first hand tool for measuring the redox behavior, electron transfer kinetics as well as determining the electron stoichiometry of any system.[31] CV is used widely to characterize the performance of various electrical energy storage devices, such as electrochemical capacitors, batteries and fuel cells.[22,31] CV of the Au-SnO_2 and P-SnO_2 photoelectrodes in the dark and under visible light irradiation were recorded at a scan rate of 50 mV/s in the range of −1.0 V to +1.0 V, as shown in Fig. 6(a),[22] CV of the Au-SnO_2 and P-SnO_2 photoelectrodes in the dark exhibited a significantly lower anodic and cathodic current, whereas the Au-SnO_2 photoelectrode exhibited a higher anodic and cathodic current under visible light irradiation compared to P-SnO_2. A prominent anodic and cathodic peak was observed at approximately −0.45 V and −0.02 V, respectively. This highlights the capacitive behaviour of the Au-SnO_2 photoelectrode, which is supposed to be induced by visible light because of the AuNPs decoration at the SnO_2 surface. In addition, the shapes of the CV curves of the Au-SnO_2 and P-SnO_2 photoelectrodes remained unchanged when irradiated with light, except for the magnitude of the anodic and cathodic current, which indicated the high stability of the Au-SnO_2 nanocomposite and highlighted the role of the AuNPs decoration of the SnO_2 surface. The increased anodic and cathodic current of the Au-SnO_2 nanocomposite under visible light irradiation reveals increased capacitance behaviour. Therefore, the enhanced capacitive performance of the Au-SnO_2 photoelectrode can be attributed to its improved charge storing ability under visible light irradiation, which is the result of the decoration of the AuNPs at the SnO_2 surface.

DPV is normally used to better understand the charge storage capability of nanomaterials and is often used as a complementary technique to CV.[10,23] DPV was performed on the Au-SnO_2 nanocomposite and P-SnO_2 nanoparticles to better understand their charging behaviour under visible light irradiation.[11,23,32] Fig. 6b shows well resolved CV peaks for the Au-SnO_2 nanocomposite and P-SnO_2 nanoparticles, which were obtained at approximately -0.34 V, corresponding to the anodic peaks. The increase in the peak current of the Au-SnO_2 nanocomposite under visible light irradiation confirmed the enhanced and excellent charge storage properties compared to P-SnO_2. Fig. 6b presents the well-defined quantized capacitance charging peaks for Au-SnO_2 nanocomposite under visible light irradiation. This was attributed to the enhanced visible light-induced photoelectrochemical activities of the Au-SnO_2 nanocomposite, which is believed to be due to the surface coating of SnO_2 by the AuNPs.[23,32] Therefore, these electrons stored at the nanocomposite can be used for different photoactive devices.

EIS was performed in the dark and under visible light irradiation to understand the transport properties of the Au-SnO_2 nanocomposite as a photoelectrode. Fig. 7a shows the EIS Nyquist plot of the Au-SnO_2 nanocomposite and P-SnO_2 nanoparticles. The complex impedance plot is presented as Z'_{real} vs. Z''_{imag}, which originates from the resistance and capacitance component of the electrochemical cell. In general, the typical Nyquist plots include one or more semicircular arcs with the diameter along the Z'_{real} axis. The semicircular arc observed in the high and low frequency regions correspond to an electron-transfer process, and its diameter represents electron transfer or charge transfer resistance.[21,33] In the present study, a semicircular arc with a smaller diameter for the Au-SnO_2 nanocomposite was obtained compared to P-SnO_2, indicating a fast electron-transfer process in the case of the Au-SnO_2 nanocomposite.[21] In particular, the smaller radius of the arc in the EIS spectra indicates a smaller electron transfer resistance at the surface of the photoelectrodes, which normally corresponds to faster interfacial charge transfer. The smaller arc radius of the EIS Nyquist plots for the Au-SnO_2 nanocomposite (Fig. 7a) compared to P-SnO_2 under visible light irradiation, indicates faster interfacial charge transfer at the Au-SnO_2 nanocomposite. The performance of Au-SnO_2 nanocomposite was found better than the previously reported other nanocomposites.[18,27] These results show that the interfacial interaction between Au and SnO_2 effectively enhances the visible light-induced charge transfer efficiency of the Au-SnO_2 nanocomposite. The EIS findings further confirmed that the Au-SnO_2 nanocomposite can be used as an effective material for visible light active photoelectrodes.

LSV was performed in the dark and under visible light irradiation to provide further evidence for the visible light-induced activities of the Au-SnO_2 nanocomposite.[34] Fig. 7b shows the LSV plots of the Au-SnO_2 nanocomposite and P-SnO_2 nanoparticles under visible light irradiation, in which the Au-SnO_2 nanocomposite showed an enhanced photocurrent than P-SnO_2. The AuNPs decorated on the SnO_2 surface can absorb visible light and generate more photoelectrons due to the SPR phenomenon. The enhancement in the photocurrent showed an increase in the visible light-induced carrier transport rate. The creation of a Schottky junction at the metal-metal oxide interface can also separate the photoelectrons and

holes, and thus increase the photocurrent.[18,27,34] Moreover, the extent of the increase in the photocurrent shown by Au-SnO_2 is also supported by the PL measurements (Fig. 2b). The results also showed that the AuNPs can harvest visible light efficiently and enhance the charge transfer activity of the Au-SnO_2 nanocomposite. It was also found that the Au-SnO_2 nanocomposite showed ~15.00, 2.70, and 1.45 times higher photocurrent than the P-SnO_2, Ag-SnO_2, Au-CeO_2 nanocomposite, respectively, under visible light irradiation. Finally, these results showed that the Au-SnO_2 nanocomposite could be used as an effective material for photocurrent, capacitance, and optoelectronic devices.

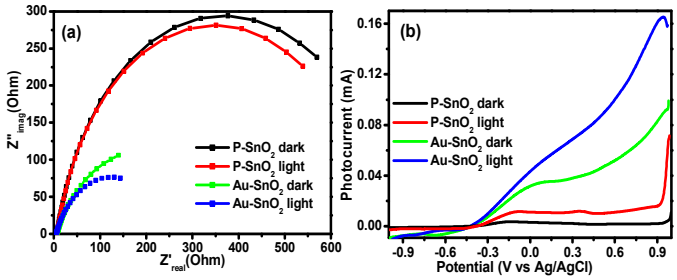

Fig. 7 Visible light-induced response of **(a)** EIS Nyquist plot, and **(b)** Photocurrent measurements by LSV for the Au-SnO_2, and P-SnO_2 photoelectrodes in the dark and under visible light irradiation.

The enhanced visible light-induced photoelectrochemical (CV, DPV, EIS and LSV) performance by the Au-SnO_2 nanocomposite confirmed that the AuNPs were well dispersed over the SnO_2 surface. The interfacial interaction and charge transfer between the AuNPs and SnO_2 could be responsible for the enhanced visible light-induced photoelectrochemical activities of the Au-SnO_2 nanocomposite. This was attributed to the enhanced charge storing and capacitance characteristics of the Au-SnO_2 nanocomposite. Based on the above enhanced visible light-induced activities shown by the Au-SnO_2 nanocomposite, the visible light-induced photocatalytic degradation of CR and MB was performed in the presence of the Au-SnO_2 nanocomposite.

Visible light-induced photocatalysis of dyes

Few studies have reported the photodegradation of dyes using the Au-SnO_2 nanocomposite, in which the UV light excites the SnO_2 semiconductor absorption band directly.[17] Few articles have reported the visible light photocatalytic activity of the Ag@SnO_2 nanocomposites, where surface plasmons of metals were utilized.[18] On the other hand, the possibility of using the surface plasmon band of AuNPs (from 500 to 550 nm) to excite the Au-SnO_2 nanocomposite photochemically (visible light) has mostly gone unnoticed. This article reports the visible light-induced photocatalytic degradation activity of the Au-SnO_2 nanocomposite using the surface plasmon band of AuNPs for CR and MB. The main advantage of this study is that AuNPs have a dual function: *first,* as a visible light harvester thereby injecting electrons into the semiconductor conduction band; and *second*, as catalytic sites for $^{\bullet}OH$ formation.[17,18,27]

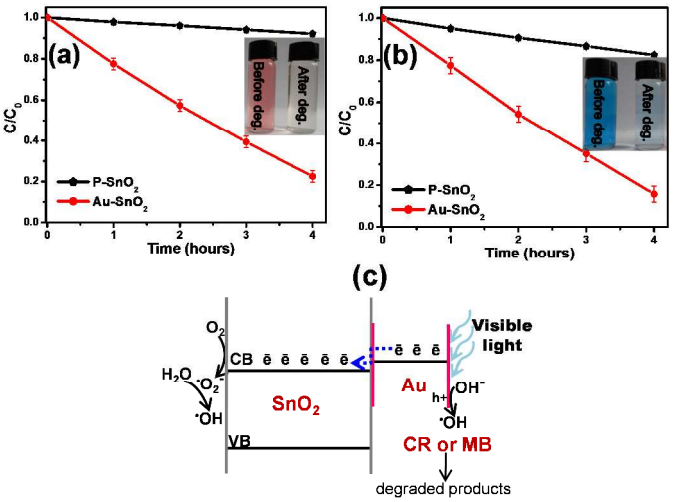

Fig. 8 Visible light-induced photocatalytic degradation of **(a)** CR, **(b)** MB in presence of the Au-SnO_2 nanocomposite and P-SnO_2 nanoparticles, and **(c)** Proposed mechanism for the visible light-induced photocatalytic degradation of CR and MB in the presence of the Au-SnO_2 nanocomposite.

A photocatalytic experiment for the degradation of CR and MB using Au-SnO_2 nanocomposite as catalyst was performed under visible light irradiation. The dye degradation experiments showed (Fig. 8a and b) that the Au-SnO_2 nanocomposite exhibited better visible light-induced photocatalytic activity for CR and MB than the P-SnO_2; approximately 10 and 6 times higher than that of the P-SnO_2, respectively, though the surface area of P-SnO_2 (38.35 m^2/g) is more than the Au-SnO_2 nanocomposite (30.11 m^2/g).[4] The experimental results showed that the Au–SnO_2 nanocomposite can effectively inhibit charge recombination and direct the charge carriers to interfacial reactions.[17,27] Charge separation was also observed by the decrease in PL intensity (Fig. 2b) of the Au-SnO_2 photocatalyst compared to P-SnO_2. Fig. 8c shows the proposed mechanism for the degradation of CR and MB using the Au-SnO_2 nanocomposite under visible light irradiation. The AuNPs at SnO_2 are believed to play essential roles in enhancing the photocatalytic activity because they can trap electrons, improve the electron–hole separation efficiency and enhance the visible light absorption, which are all beneficial for enhancing the visible light-induced photocatalytic activity of the Au-SnO_2 nanocomposite.[27,35,36] The AuNPs in contact with SnO_2 facilitates electron−hole separation, and then assists in the formation of hydroxyl radicals.[17,27,35,36] The hydroxyl radicals ($^{\bullet}OH$) and superoxide radical anions ($^{\bullet}O_2^-$) produced under visible light irradiation might be responsible for decomposing the dyes.[17,18,27,37] In general, photogenerated electrons can react with the oxygen molecules adsorbed on the surface of the Au-SnO_2 photocatalyst to yield $^{\bullet}O_2^-$. Therefore, the Au-SnO_2 photocatalyst showed enhanced visible light-induced photocatalytic activity compared to P-SnO_2. Finally, these results suggest that AuNPs at the SnO_2 surface will help the formation of $^{\bullet}OH$ and $^{\bullet}O_2^-$ reactive radicals, and simultaneously assist in the degradation of the dyes. It was observed that in comparison to the previous studies, the Au-SnO_2 nanocomposite exhibited much better and faster visible-

light induced photocatalytic degradation of the organic pollutants than the Ag-SnO_2 and Au-CeO_2 nanocomposite.[18,27] This is attributed to the better interfacial interaction between Au and SnO_2 and increased charge separation in Au-SnO_2 nanocomposite. Overall, the Au-SnO_2 nanocomposite can also be used as a visible light active photocatalyst for environmental remediation.

The advantage of this synthetic procedure is that deionized water was used as a solvent, which does not have any adverse effects on the surroundings and environment. This protocol does not involve any expensive materials or devices and energy input except for the routine instruments. The Au-SnO_2 nanocomposite obtained was quite stable in the reaction mixture as well as after isolation from the reaction mixture in the solid state to air and moisture. This allows smooth handling for a range of applications. Moreover, it was a controlled synthesis. Considering the interest in gold catalysis, these findings may open new avenues for the application of this type of photocatalyst to visible light-induced photocatalysis and other visible light active devices.

Stability of the Au-SnO_2 nanocomposite

The stability of the Au-SnO_2 nanocomposite was evaluated by sonicating the aqueous suspension of Au-SnO_2 nanocomposite for 1 h. The centrifuged solution was later monitored for any leached gold using an UV−visible spectrophotometer (Fig. S7). This investigation did not show any absorbance in the 500-550 nm range for gold. This confirms that the Au-SnO_2 nanocomposite was stable.

Conclusions

Au-SnO_2 nanocomposite was synthesized using an electrochemically active biofilm and its visible light-induced photoelectrochemical and photocatalytic degradation properties were examined. The photoelectrochemical studies of the Au-SnO_2 nanocomposite under visible light irradiation showed enhanced activities compared to the P-SnO_2. Cyclic voltammetry, differential pulse voltammetry, electrochemical impedance spectroscopy, and linear sweep voltammetry verified that Au-SnO_2 nanocomposite showed a better response under visible light irradiation. Cyclic voltammetry, differential pulse voltammetry, electrochemical impedance spectroscopy, and linear sweep voltammetry confirmed the capacitance and quantized capacitance charging behavior of the Au-SnO_2 nanocomposite. Linear sweep voltammetry further confirmed the enhancement in photocurrent generated by the Au-SnO_2 nanocomposite under visible light irradiation. The photocatalytic degradation studies revealed the enhanced visible light-induced degradation of congo red and methylene blue by the Au-SnO_2 nanocomposite compared to the P-SnO_2 nanoparticles. Overall, the as-synthesized Au-SnO_2 nanocomposite can be used as an effective material for visible light-induced devices and as photocatalyst, which opens up new possibilities for the synthesis and applications of similar novel nanomaterials.

Acknowledgements

This work was supported by Priority Research Centers Program through the National Research Foundation of Korea (NRF) funded by the Ministry of Education (2014R1A6A1031189).

Notes and references

[1]*School of Chemical Engineering and* [2]*Center for Research Facilities, Yeungnam University, Gyeongsan-si, Gyeongbuk 712-749, South Korea. Phone: +82-53-810-2517; Fax: +82-53- 810-4631.*
***Corresponding Author Email:** mhcho@ynu.ac.kr*
¥***Co-corresponding Author Email:** mmansoobkhan@yahoo.com*

†Electronic Supplementary Information (ESI) available: [UV-vis DRS spectra, XRD patterns of Au-SnO_2, SAED, HAADF and EDX of Au-SnO_2, UV-vis spectra of Au-SnO_2 for Au leaching] See DOI: 10.1039/b000000x/

1 H. Wang and A. L. Rogach, *Chem. Mater.*, 2014, **26**, 123−133.
2 S. A. Papargyri, D. N. Tsipas, D. A. Papargyris, A. I. Botis and A. D. Papargyris, *Solid State Phenomena*, 2005, **106**, 57–62.
3 J. S. Chen and X. W. Lou, *Small,* 2013, **9**, 1877–1893.
4 S. A. Ansari, M. M. Khan, M. O. Ansari, J. Lee and M. H. Cho, *New Journal of Chemistry*, 2014, **38**, 2462–2469.
5 G. Oldfield, T. Ung and P. Mulvaney, *Adv. Mater.*, 2000, **12**, 1519–1522.
6 M. M. Khan, S. Kalathil, T. H. Han, J. Lee and M. H. Cho, *J. Nanosci. Nanotechnol.*, 2013, **13**, 6079–6085.
7 T. H. Han, M. M. Khan, S. Kalathil, J. Lee and M. H. Cho, *J. Nanosci. Nanotechnol.*, 2013, **13**, 6140–6144.
8 M. M. Khan, J. Lee and M. H. Cho, *Int. J. Hydrogen Energy*, 2013, **38**, 5243–5250.
9 M. Brust and G. J. Gordillo, *J. Am. Chem. Soc.*, 2012, **134**, 3318−3321.
10 R. W. Murray, *Chem. Rev.*, 2008, **108**, 2688–2720.
11 S. Kalathil, J. Lee and M. H. Cho, *ChemSusChem*, 2013, **6**, 246–250.
12 K. K. Haldar and A. Patra, *Chemical Physics Letters*, 2008, **462**, 88–91.
13 Y. T. Yu and P. Dutta, *Sens. Actuators B*, 2011, **157**, 444–449.
14 F. C. Chung, R. J. Wua and F. C. Cheng, *Sens. Actuators B*, 2014, **190**, 1–7.
15 K. Yu, Z. Wu, Q. Zhao, B. Li, and Y. Xie, *J. Phys. Chem. C*, 2008, **112**, 2244–2247.
16 T. Yanagimoto, Y. T. Yu and K. Kaneko, *Sens. Actuators B*, 2012, **166–167**, 31–35.
17 W. Wu, L. Liao, S. Zhang, J. Zhou, X. Xiao, F. Ren, L. Sun, Z. Dai and C. Jiang, *Nanoscale*, 2013, **5**, 5628–5636.
18 S. A. Ansari, M. M. Khan, M. O. Ansari, J. Lee and M. H. Cho, *RSC Adv.*, 2014, **4**, 26013–26021.
19 L. Xian, Z. Jiamin, Y. Xinli, D. Weilin and F. Kangnian, *Chinese Journal of Catalysis*, 2013, **34**, 1013–1019.
20 Y. T. Yu and P. Dutta, *J. Solid State Chem.*, 2011, **184**, 312–316.
21 F. Li, J. Song, H. Yang, S. Gan, Q. Zhang, D. Han, A. Ivaska and L. Niu, *Nanotechnology*, 2009, **20**, 455602 (6pp). doi:10.1088/0957-4484/20/45/455602.

22 N. L. Wu, J. Y. Hwang, P. Y. Liu, C. Y. Han, S. L. Kuo, K. H. Liao, M. H. Lee, and S. Y. Wang, *J. Electrochem. Soc.*, 2001, **148**, A550-A553.
23 A. Yang, Y. Xue, Y. Zhang, X. Zhang, H. Zhao, X. Li, Y. He and Z. Yuan, *J. Mater. Chem. B*, 2013, **1**, 1804–1811.
24 M. M. Khan, S. A. Ansari, J. H. Lee, J. Lee, M. H. Cho, *ACS Sustainable Chem. Eng.,* 2014, **2**, 423−432.
25 T. H. Han, M. M. Khan, S. Kalathil, J. Lee and M. H. Cho, *Ind. Eng. Chem. Res*., 2013, **52**, 8174–8181.
26 J. Liqiang, Q. Yichun, W. Baiqi, L. Shudan, J. Baojiang, Y. Libin, F. Wei, F. Honggang, S. Jiazhong, *Sol. Energy Mater. Sol. Cells*, 2006, **90**, 1773−1787.
27 M. M. Khan, S. A. Ansari, M. O. Ansari, B. K. Min, J. Lee, and M. H. Cho, *J. Phys. Chem. C*, 2014, **118**, 9477−9484.
28 B. D. Cullity, S. R. Stock, Elements of X-ray Diffraction; Prentice Hall, NJ, **2001**.
29 S. Gubbala, H. B. Russell, H. Shah, B. Deb, J. Jasinski, H. Rypkema and M. K. Sunkara, *Energy Environ. Sci.*, 2009, **2**, 1302–1309.
30 M. Murdoch, G. I. N. Waterhouse, M. A. Nadeem, J. B. Metson, M. A. Keane, R. F. Howe, J. Llorca and H. Idriss, *Nature Chemistry*, 2011, **3**, 489–492.
31 H. Wang and L. Pilon, *Electrochimica Acta*, 2012, **64**, 130–139.
32 M. M. Khan, S. A. Ansari, J. Lee, and M. H. Cho, *J. Ind. Eng. Chem.*, 2013, **19**, 1845–1850.
33 W. H. Leng, Z. Zhang, J. Q. Zhang and C. N. Cao, *J. Phys. Chem. B*, 2005, **109**, 15008−15023.
34 J. Gan, X. Lu, J. Wu, S. Xie, T. Zhai, M. Yu, Z. Zhang, Y. Mao, S. C. Wang, Y. Shen, Y. Tong, *Sci. Rep.*, 2013, **3**, 1021−1028.
35 C. G. Silva, R. Juarez, T. Marino, R. Molinari, H. Garcia, *J. Am. Chem. Soc.*, 2011, **133**, 595–602.
36 S. Banerjee, S. C. Pillai, P. Falaras, K. E. O'Shea, J. A. Byrne, and D. D. Dionysiou, *J. Phys. Chem. Lett.*, 2014, **5**, 2543−2554.
37 Z. Li, G. Duan, G. Liu, Z. Dai, J. Hu, W. Cai and Y. Li, *J. Mater. Res.*, 2014, **29**, 115−122.

Table of Contents (TOC)

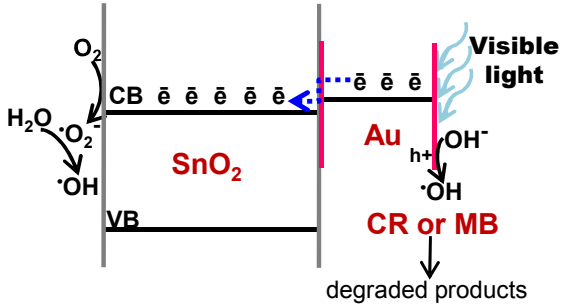

Visible light-induced photocatalytic degradation of colored dyes using Au-SnO_2 nanocomposite.